Effect of Dead Volumes on the Performance of an Industrial-Scale Simulated Moving-Bed Parex Unit for *p*-Xylene Purification

Marta S. P. Silva and Alírio E. Rodrigues
Dept. de Engenharia Química, Faculdade de Engenharia, LSRE - Laboratory of Separation and Reaction Engineering, Universidade do Porto, 4200-465 Porto, Portugal

José P. B. Mota
LAQV, REQUIMTE, Dept. de Química, Faculdade de Ciências e Tecnologia, Universidade Nova de Lisboa, 2829-516 Caparica, Portugal

DOI 10.1002/aic.15022
Published online September 15, 2015 in Wiley Online Library (wileyonlinelibrary.com)

The cyclic steady state (CSS) of the industrial-scale, seven-zone, simulated moving-bed (SMB) unit for p-xylene (p-x) purification (Parex unit) with three types of dead volumes—bed lines, push-around and pump-around circulation lines, and bed heads—is analyzed. In particular, the effects of the size and level of hydrodynamic dispersion of each dead volume on process performance and on its CSS are studied in detail. The circulation lines change the CSS behavior from t^*-periodic to Nt^*-periodic, where t^* is the switching interval and $N=12$ is the number of columns in each adsorbent chamber. A high level of axial dispersion in the bed lines, characterized by Péclet numbers smaller than 100, affects the p-x purity. Moreover, the bed lines lower the average p-x concentration in the extract, which reduces the p-x recovery. If the small time lags introduced by the circulation lines are neglected, it is possible to develop a detailed process model that considers the operation of the Parex unit over a single switching interval as opposed to a full cycle, and whose CSS solution can be efficiently computed using a full-discretization approach. Finally, it is shown that the volume of the bed heads influences significantly the performance of the Parex unit, and that its impact on the location of the operating point with respect to the boundaries of the separation region can be approximately taken into account using the standard true moving-bed-SMB equivalence rules if they are corrected for the presence of extra interparticle fluid.
 AIChE J, 62: 241–255, 2016
Keywords: simulated moving bed, Parex, p-xylene, dead volumes

Introduction

BTX aromatics (benzene, toluene, and xylenes) are mainly produced from reformate, pyrolysis gasoline, and coke oven light oil. In the catalytic reforming, a straight run or hydrocracker naphtha cut with a low-octane index is converted into high-octane aromatics: benzene, mixed xylenes (*p*-xylene, *p*-x; *m*-xylene, *m*-x; *o*-xylene, *o*-x; and ethylbenzene, eb), and toluene (tol). The reformate contains a variable amount of xylenes, usually in the range 18–33%-v/v, depending on the operating conditions of the reformer, type of catalyst being used, and type of processed crude oil. Pyrolysis gasoline is obtained from stream cracking as a by-product and it contains approximately 20% of mixed xylenes. In the case of xylene production from coal, carbonization at high temperature leads to the production of light oil with 3–6%-v/v of mixed xylenes. The production of xylenes from coke oven light oil has the lowest yield of these three production methods. It should be mentioned that xylenes can also be produced by toluene disproportionation. This catalytic process is usually more expensive than the production from reformate or pyrolysis gasoline; however, the product obtained by the former method has a higher purity and the production of eb is almost eliminated.[1,2]

The *p*-x aromatic is commonly separated from other xylenes and eb through crystallization[1–6] and/or adsorption.[1,2,7–11] The first licensed adsorption process for the separation of *p*-x was the Parex process.[7,12–16] Broughton and Gerhold[12] first patented this process in 1961, assigned by Universal Oil Products (UOP), and introduced the simulated moving-bed (SMB) technology for the continuous separation of *p*-x by adsorption. In the SMB technology, the differences in affinity of the various components of the feed for the adsorbent are explored by simulating the countercurrent contact between the solid and the liquid. As its development, the SMB technology has been preferentially chosen over crystallization for the separation of *p*-x.[17]

The SMB technology results from the practical implementation of the true moving-bed (TMB) concept, where the solid moves countercurrently with respect to the liquid.[18] To avoid the difficulty of experimentally realizing the plug flow of the

Correspondence concerning this article should be addressed to A. E. Rodrigues at arodrig@fe.up.pt.

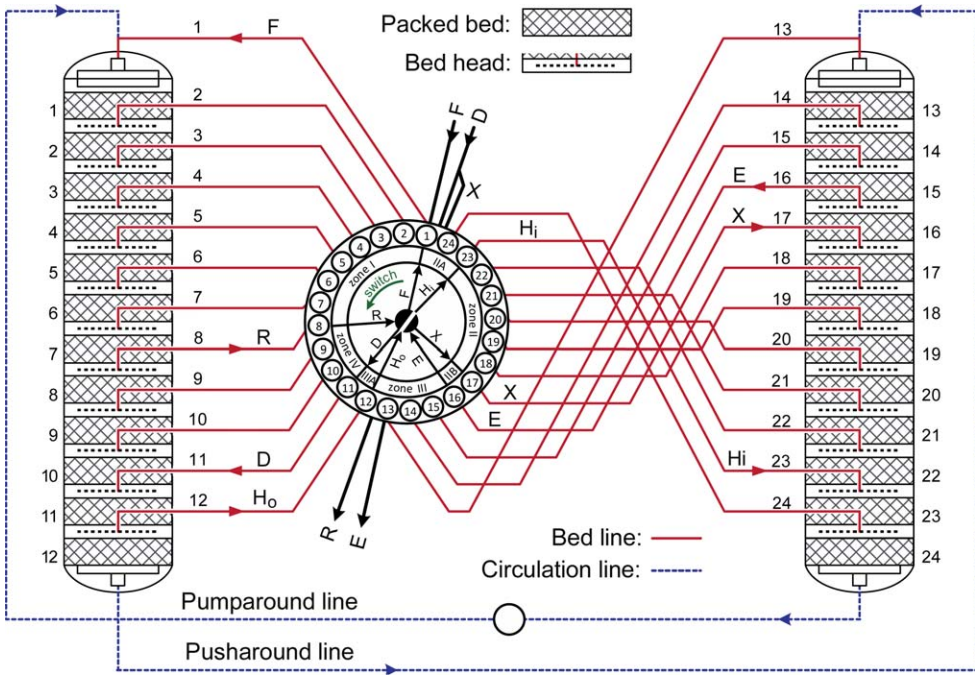

Figure 1. Schematic of the Parex unit, with 12 columns per adsorbent chamber connected to a single rotary valve, organized in a seven-zone configuration.

Notation: D, adsorbent; E, extract; F, feed; H_i, primary flush-in; H_o, primary flush-out; R, raffinate; X, secondary flush or recycle. [Color figure can be viewed in the online issue, which is available at wileyonlinelibrary.com.]

solid and the problems related to the abrasion of the equipment and formation of fines due to the friction between the adsorbent particles, the SMB does not move the solid but instead simulates its movement by periodically and synchronously switching the four ports (raffinate, extract, feed, and desorbent) in the direction of the fluid flow. The port switching is implemented by means of a rotary valve[14] in all of UOP's SMB-type processes[19]; the rotary valve is connected to all beds and redirects the inlet and outlet streams of the process.

Two strategies can be, and have been, used to build the model of a SMB unit. One strategy is to mimic the real operation of the unit that periodically switches the positions of the inlet and outlet streams or the columns[20]; the other strategy is based on an equivalent TMB model.[21] The results obtained with the TMB model are close to the SMB model when the number of columns is large and the switching time and the column length are small enough.[22]

The main difference between the SMB and TMB models is the stationary regime under which the unit operates. In the SMB model, the countercurrent motion of the solid is simulated by the periodic, discrete jump of the injection and collection points by one column in the direction of the fluid flow; as a result, the periodic movement of the inlet/outlet ports generates a cyclic steady state (CSS) instead of a true steady state as in the TMB. Once the CSS is reached after a sufficiently large number of cycles, the time-dependent behavior of the SMB during each switching interval is repeated exactly over the next. The concentrations of all components in the extract but the desorbent decrease, while the concentrations of all components in the raffinate but the desorbent increase; however, under CSS conditions, the time-averaged concentration over a switching interval is time-independent and is close to the concentration given by the equivalent TMB model.

These considerations about the equivalence between the TMB and the SMB are valid when the dead volumes of the real SMB unit can be neglected or the dead volumes are uniformly distributed over the ring of columns and the system is operated under linear adsorption conditions. This is not the case for the Parex unit as it has different types of nonuniformly distributed dead volumes and is operated under overloaded, nonlinear conditions.[20]

The Parex unit has 24 columns divided into two adsorbent chambers, as shown in the schematic diagram depicted in Figure 1. A dead volume—the circulation line—connects the downstream end of one chamber to the upstream end of the other. The fluid is transferred between the 24 beds and the rotary valve through 24 bed lines that act as 24 dead volumes where the fluid is held back whenever the line is not being used. The flow distributor and collector and the support grids in each bed, altogether called bed-head dead volumes, also introduce a dispersive time lag.

The SMB unit implemented in the commercial Parex process has seven zones, instead of the typical four zones.[23–29] The three extra zones avoid the contamination of streams flowing in the lines during subsequent switching intervals. The zone configuration of the Parex's rotary valve is 7-2-6-1-4-1-3 [*I*, *IIA*, *II*, *IIB*, *III*, *IIIA*, and *IV*]; the equivalent four-zone configuration would be 7-9-5-3. This zone numbering follows the convention adopted by Silva et al.[20] Appendix A gives a more detailed description of the different types of dead volumes and summarizes the purpose and workings of the extra flushing streams; overall, this appendix and the information given in Ref. 20 provide a comprehensive description of the commercial Parex process.

One consequence of implementing a SMB process by means of a rotary valve, as is the case in the Parex process, is that the bed lines, through which the fluid is transferred back and forth between the adsorbent chambers and the rotary valve, are dead volumes that cause stream contamination.[20–30] If the unit is described with only the classical four zones, the

Table 1. Summary of the Simulation Parameters for the Case Study of an Industrial-Scale Parex Unit

Construction and Adsorbent	Rotary Valve	Configuration (*I-IIA-II-IIB-III-IIIA-IV*): 7-2-6-1-4-1-3		Equilibrium, Kinetics, and Axial dispersion		k (s^{-1})	K (dm^3/mol)	q_m (mol/kg)
	Column	Column diameter, D (m)	4.27					
		Length of one bed, L (m)	0.91		*p*-xylene	0.08	295.3	1.256
		Porosity, ε	0.39		*m*-xylene	0.08	20.82	1.202
	Particle	Particle porosity, ε_p	0.36		*o*-xyleneethylbenzene	0.08	25.45	1.224
		Particle density, ρ_p (kg/m^3)	1480		*p*-diethylbenzenenonaromaticstoluene	0.08	38.71	1.181
		Particle radius, R_p (mm)	0.31			0.07	860.1	0.703
	Bed lines	Diameter, D (m)	0.127			0.07	0	0
		Length, L (m)	17.8			0.08	191.2	1.213
	Circulation lines	Diameter, D (m)	0.203					
		Length, L (m)	25.0					
	Bed head dead volume	Diameter, D (m)	4.27					
		Length, L (m)	0.22					
	Adsorbent	Selective volume, V_s (m^3)	48.1					
		Nonselective volume, V_w (m^3)	239.7					
	Unit/project	Feed project, $Q_F^{project}$ (m^3/h)	107.5		*Pe*	1000	$\boldsymbol{Pe_{dead}}$	200

Operation	Feed in Relation to Project, $f_F^{project}$	A/Q_F^a	L_2/A	L_3/A	L_4/A	Aromatic in Relation to Feed, f_F^a	Line Wash Flush, f_H^{line}	Line Wash Recycle, f_X^{line}	Feed (wt %)						
									p-x	*m*-x	*o*-x	eb	n/a	tol	benz
	0.95	0.708	0.798	1.56	−0.35	0.940	1.3	1.1	18.92	44.08	13.86	11.99	10.80	0.34	0.01

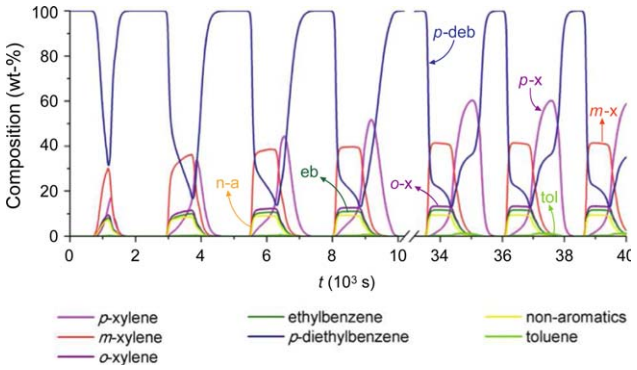

Figure 2. Temporal composition profile (wt %) monitored in the pump-around line starting from an initial state where the unit is filled with *p*-deb until CSS is achieved.

The plant operation information is given in Table 1 and in the leftmost data column of Table 2. [Color figure can be viewed in the online issue, which is available at wileyonlinelibrary.com.]

effect of the bed lines is neglected. However, when the Parex unit is modeled with seven zones, the bed lines and their effect must be taken into account.

If the SMB approach is considered, the dead volumes of the bed heads and the dead volumes of the circulation lines can also be included in the model. It is important to note that it is not straightforward to correctly include dead volumes in the ideal TMB model, as their inclusion would imply considering an unrealistic solid by-pass between columns. Nevertheless, the impact of the bed-head volumes and circulation lines on the location of the operating point with respect to the boundaries of the separation region can be approximately accounted for by correcting the standard TMB-SMB equivalence rules for the presence of extra interparticle fluid.

In this work, the CSS of an industrial-scale Parex unit with dead zones and three types of dead volumes is analyzed in detail. The effect of the different types of dead volumes on the performance of the industrial unit is assessed and the simplifying assumptions that reduce the detailed Parex model to a more computationally efficient one yet retaining all of the essential properties of the former are discussed.

Parex Process, Simulation Model, and Numerical Solution

The detailed description of the Parex unit and the mathematical model are given elsewhere.[20] The SMB model is based on 24 instances—one for each column—of a multicomponent fixed-bed submodel.[31] The fixed-bed submodel assumes isothermal conditions, axially dispersed plug flow with all mass-transfer resistances lumped under the form of a linear driving force,[32] incompressible flow with constant velocity along the bed, and no radial dispersion. The small contribution from radial dispersion, if any, is lumped into the various axial dispersion coefficients considered in the model.

The SMB model also takes into account the three types of dead volumes: bed lines, circulation lines, and bed heads. Both the bed lines and circulation lines are described by axially dispersed plug-flow models; it is worth noting that in the case of the bed lines, the instantaneous direction of the fluid flow depends on whether the stream is being injected or withdrawn. The bed-head dead volumes are modeled as perfectly mixed stirred tanks.

The implementation of the SMB model in gPROMS 3.3.1 (Process System Enterprise, London, UK) is explained elsewhere.[20] Briefly, the mathematical model was reduced to a system of ordinary differential and algebraic equations in time by discretizing the axial domains using third-order orthogonal collocation on finite elements. The resulting system was then integrated in time by the gPROMS's DASOLV solver with a relative error tolerance of 10^{-5}. The fixed-bed submodel, the bed lines, and the circulation lines were discretized into 5, 21, and 37 uniform finite elements, respectively.

This work focuses on the analysis of the industrial case study C reported by Silva et al.,[20] whose input parameters are summarized in Table 1. It is worth noting that this work is one of very few in which simulations are compared against real industrial plant data and where the dead volumes are discussed in light of the design and operating parameters defined by the licensor.

Influence of the Dead Volumes on the Performance of the Parex Unit

For the case study defined in Table 1, the simulations started from an initial condition where the unit is initially filled with *p*-deb. Figure 2 shows the evolution over time of the concentrations in the pump-around line until CSS is achieved. The CSS is reached after ca. 12 cycles. The time-periodic concentration profiles repeat every $24t^*$ time units (24×106.3 s$=2551.2$ s) because they are sampled at a fixed point (pump-around line) of the Parex unit.

The evolution in time of the concentrations in the extract and raffinate streams is shown in Figures 3 and 4. The temporal profile of the extract composition over a switching interval is shown in detail in Figures 3c, d and that of the raffinate composition is depicted in Figures 4c, d; these profiles were recorded under CSS conditions. During the residence time of a bed line, the extract has the same composition as the stream that was held back in the bed line (secondary flush composition) from which the extract is withdrawn. In the case under study, the residence time of the bed line is $V_{line}/Q_E = 13.6$ s; only after this time lag does the true extract concentration front reach the outlet line after crossing the rotary valve. Indeed, Figure 3c shows the expected monotonically decreasing *p*-x temporal concentration profile, but only after the first V_{line}/Q_E time units of the switching interval.

The time lag created by the bed line is also observed in the dynamics of the raffinate stream (Figure 4); in the case under study, the raffinate concentration front reaches the rotary valve $V_{line}/Q_R = 4.3$ s after the beginning of the step. The line through which the raffinate stream is collected is filled with *p*-deb, as this line was previously used to inject the desorbent stream into the system. When the raffinate composition front reaches the outlet of the unit, the concentrations of *p*-x, *m*-x, *o*-x, eb, n-a, and toluene start to increase.

The temporal profiles of the extract and raffinate concentrations plotted in Figures 3b and 4b over a full cycle under CSS conditions are almost t^*-periodic because they are sampled at positions that move with the port switching of the rotary valve. Although not readily noticeable in the visual analysis of the instantaneous concentration values, the time-averaged values (solid lines in Figures 3a and 4a and dashed lines in Figures 3b and 4b) show that the profiles are exactly $12t^*$-periodic because the pump-around and push-around circulation lines

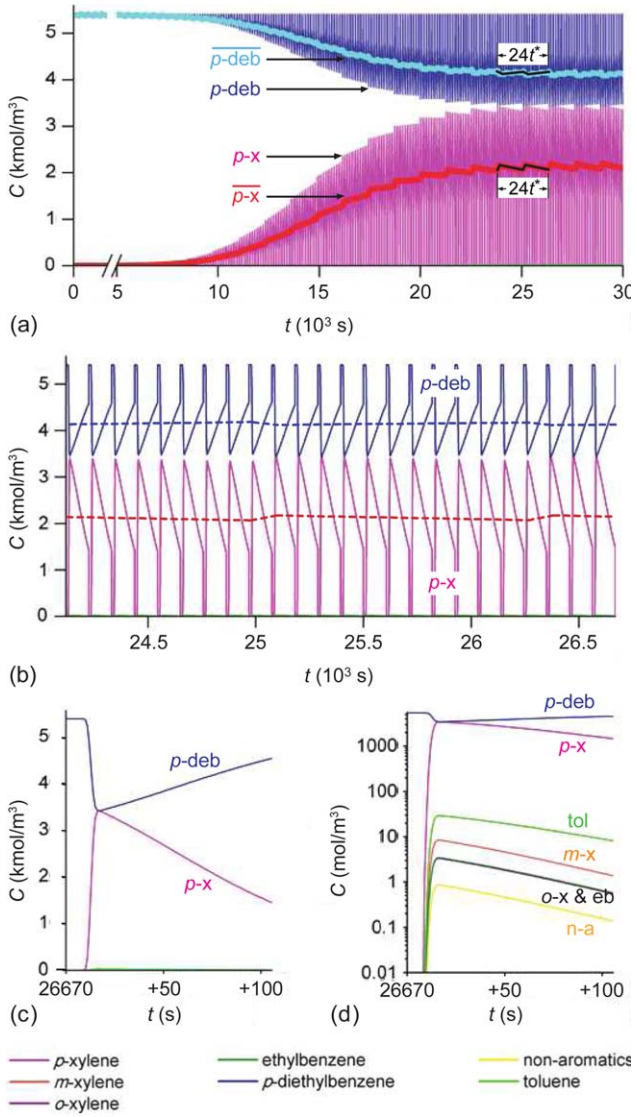

Figure 3. Analysis of the extract stream.

(a) Temporal concentration profiles (*p*-deb and *p*-x) and their t^*-averaged values ($\overline{p\text{-deb}}$ and $\overline{p\text{-x}}$); (b) temporal concentration profiles (solid lines) and their t^*-averaged values (dashed lines) for a full CSS cycle; (c and d) zoom-in of the temporal concentration profiles for a single CSS switching interval. Operating conditions given in Table 1 and in the leftmost column of Table 2. [Color figure can be viewed in the online issue, which is available at wileyonlinelibrary.com.]

break the t^*-periodicity by dividing the Parex flow sheet into two equal halves (cf. Figure 1); if the push-around and pump-around lines had very different volumes or dispersion levels, the concentration profiles would be exactly $24t^*$-periodic.

To assess the influence of the circulation lines, they were removed from the model. Figure 5a compares the temporal profiles of the average *p*-x and *p*-deb concentrations in the extract with and without circulation lines. Figures 5b, c show the extract temporal concentration profiles, in the presence and absence of circulation lines, when the extract is withdrawn through Position 1 (or 13) and Position 12 (or 24).

Figure 5a shows that in the absence of circulation lines, the extract concentration averaged over a switching interval tends toward a constant value as the CSS is approached—this value is independent of the number of elapsed switching intervals in a cycle. However, in the presence of circulation lines, the extract concentration averaged over a switching interval is $12t^*$-periodic because the circulation lines connect the two trains of 12 columns. Moreover, under CSS conditions, the t^*-averaged extract concentration of the real Parex unit approaches the t^*-averaged extract concentration of the model without circulation lines at the end of each half cycle, that is, after 12 switching intervals.

Figures 5b, c compare the variations of the concentrations in the volumes of extract withdrawn from the first and last positions of the adsorbent chamber, respectively. As the extract position moves along the adsorbent chamber, the maximum concentration of *p*-xylene in the extract achieved over the course of switching interval decreases. When the unit is simulated without circulation lines, the temporal concentration

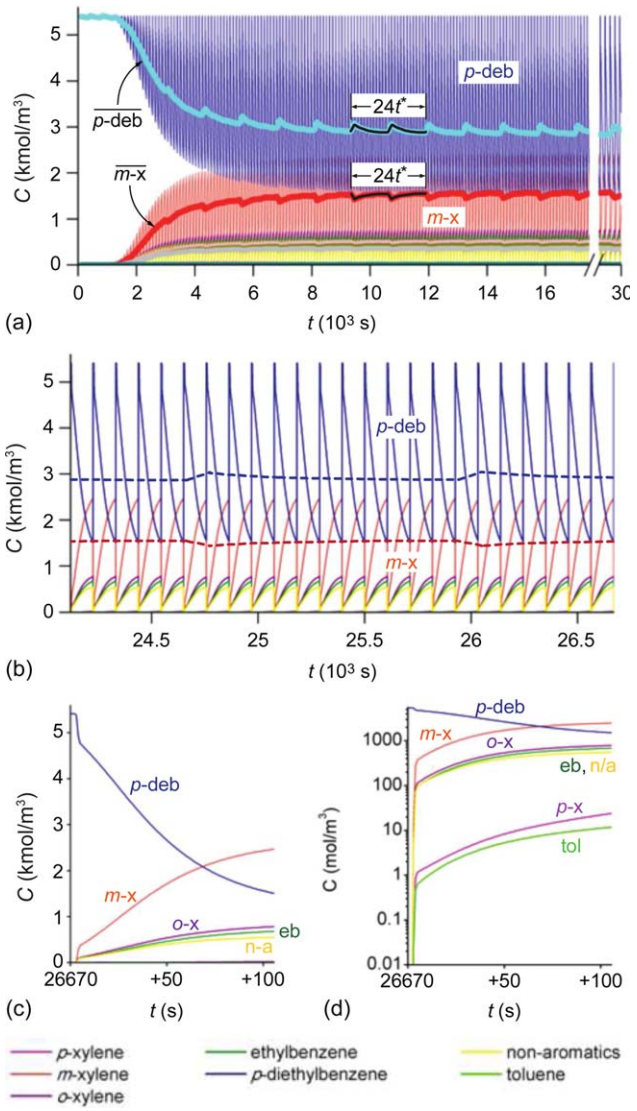

Figure 4. Analysis of the raffinate stream.

(a) Temporal concentration profiles (*p*-deb and *m*-x) and their t^*-averaged values ($\overline{p\text{-deb}}$ and $\overline{m\text{-x}}$); (b) temporal concentration profiles (solid lines) and their t^*-average values (dashed lines) for a full CSS cycle; (c and d) zoom-in of the temporal concentration profiles for a single CSS switching interval. Operating conditions given in Table 1 and in the leftmost column of Table 2. [Color figure can be viewed in the online issue, which is available at wileyonlinelibrary.com.]

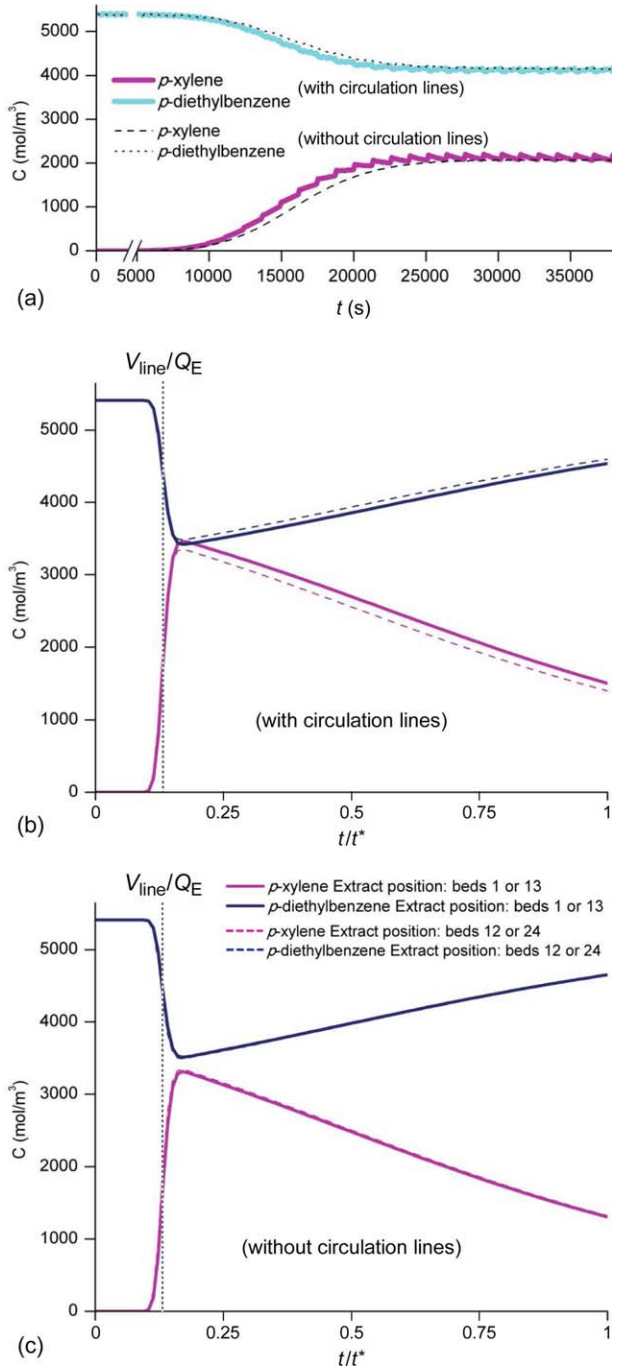

Figure 5. Temporal profile over a switching interval of the average concentration in the extract in the presence and absence of circulation lines: (a) temporal dynamics until CSS; (b) zoom-in of the profiles for a single switching interval (simulation with circulation lines); (c) zoom-in of the profiles for a single switching interval (simulation without circulation lines).

[Color figure can be viewed in the online issue, which is available at wileyonlinelibrary.com.]

of the extract for each switching interval does not change with the withdrawal position in the adsorbent chamber.

The $12t^*$-periodicity of the t^*-averaged concentration is a consequence of the delay created by the volume of the circulation lines and is not influenced by the degree of axial dispersion in the circulation lines. The lag created by the circulation lines is not constant, it depends on the zones crossing the pump-around and push-around lines. In the case under study, the lag of the circulation lines varies between 5.8 and 9.3 s; the former value is when zone *I* is crossing the lines, the latter value is when zone *IV* is crossing the lines. When the extract outlet position (EOP) is in Positions 1–4 (or 13–16), 5 (17), 6–8 (18–20), and 9–12 (21–24), the zones crossing the circulating line are, respectively, *III*, *IIIA*, *IV*, and *I*. It should be mentioned that the level of axial dispersion considered for the circulation lines ($Pe_{\text{dead}} = 200$) is not high enough to significantly influence the concentration profile at the inlet position of the adsorbent chamber, that is, the concentration profiles measured at the inlet and outlet of the circulation lines are almost coincident.

Different levels of axial dispersion were considered for the circulation and bed lines by imposing values for Pe_{dead} between 25 and 400. Figure 6a compares the product purities obtained in two cases: (1) when the same level of axial dispersion is imposed in the bed and circulation lines and (2) when the circulation lines are eliminated from the model and different levels of axial dispersion are imposed only in the bed lines. Figure 6b reports the results of a similar exercise for the case where the bed lines are eliminated from the model and different levels of axial dispersion are imposed only in the circulation lines.

Figure 6 shows that the removal of the dispersed plug-flow dead volumes improves the final product purity because the removal of a dispersed plug-flow dead volume operated at a moderate-to-large Péclet number is equivalent to reducing the total nonselective volume of the separation. For example, for a fixed value $Pe_{\text{dead}}=200$, the product purity increases from 99.65 to 99.80% when the circulation lines are removed (Figure 6a) and to 99.74% when the bed lines are removed (Figure 6b). It is also worth noting that without circulation lines, the dead volumes are more evenly distributed over the ring of 24 columns.

Figure 6a shows that the level of axial dispersion in the bed lines influences the performance of the Parex unit as a decrease in the purity is observed for Pe_{dead} values in the bed lines below ca. 100. However, in the absence of bed lines, the axial dispersion in the circulation lines does not affect the purity of the extract, as a constant value of 99.74% was obtained for $25 < Pe_{\text{dead}} < 400$. Thus, when there is a large level of axial dispersion in the dispersed plug-flow dead volumes, the removal of the bed lines has a larger beneficial impact on the final product purity than the removal of the circulation lines.

When the axial dispersion is decreased in the bed lines, the purity increases until achieving a maximum value (99.65% in the case under study). If the concentration of each component at the inlet position of the bed line were constant, one should obtain constant *p*-x purity in the extract despite the variation of the axial dispersion level, as the proportion between all components is maintained. However, the Parex unit operates under CSS conditions and, therefore, the concentration at the inlet of the bed lines varies over each switching interval. During a switching interval, the concentrations of all components (except *p*-deb) decrease at the upstream end of the bed lines (which is the same as the outlet of the adsorbent chamber) through which the extract is withdrawn, but the individual concentrations do not decrease at the same rate. An increased axial dispersion changes the time interval during which the

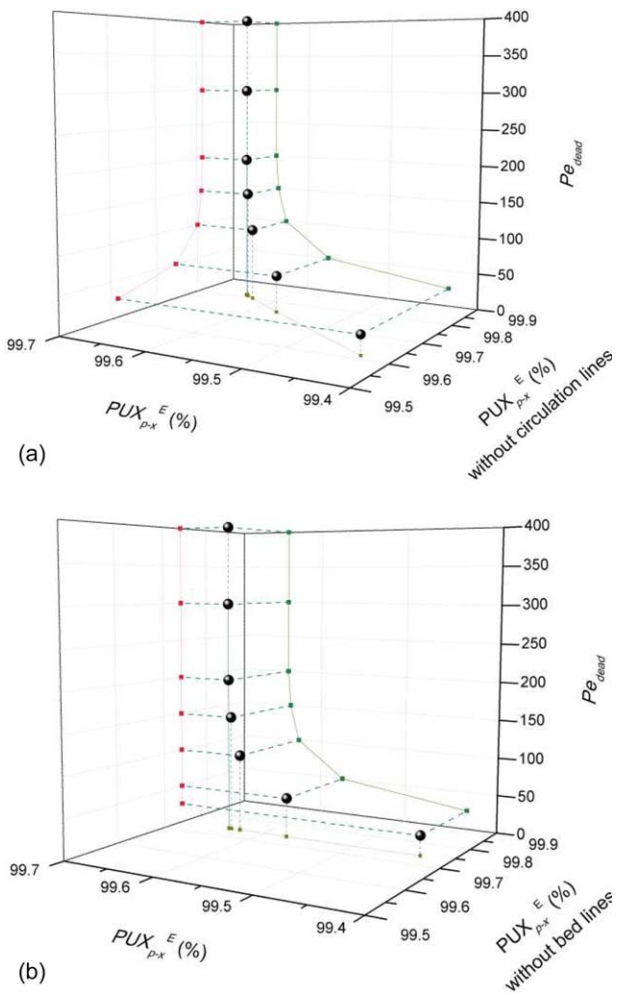

Figure 6. p-Xylene purity in the extract stream as function of the level of axial dispersion in the bed and circulation lines ($25 < Pe_{dead} < 400$) : (a) comparison with the results without circulation lines ($L_{circ} = 0$); (b) comparison with the results without bed lines ($L_{lines} = 0$).

[Color figure can be viewed in the online issue, which is available at wileyonlinelibrary.com.]

product is effectively withdrawn (anticipates the collection), and, consequently, the total amount of each component taken during a switching interval changes.

Table 2 lists the operating parameters for different volumes of the bed lines. It should be noted that for the case where the bed lines are neglected ($V_{\text{line}} = 0$), the model of the Parex unit is reduced to a SMB model with only four zones.

As the case without bed lines has different input parameters, and for that reason a different purity (99.74%), its performance cannot be strictly compared with the other cases. However, the purity increase to 99.82% observed in the absence of circulation lines can be justified. As explained above, the circulation lines create a time lag that increases the concentration of impurities (*m*-x, *o*-x, and eb) before the extract port. This is shown in Figure 7, which compares the concentration profiles for the seven-zone and four-zone configurations, with and without circulation lines, as function of the feed inlet position (FIP). For the simulation of the four-zone configurations, the zone flow rates were adjusted according to Table 2.

As discussed above, when the circulation lines are neglected, the differences in the concentration profiles are due do the delay created by the pump-around/push-around dead volumes. Figure 7 shows that when the bed lines are neglected and the model is transformed into a four-zone SMB, the concentration profiles are coincident except between FIP 1–3, 9–10, 14–15, and 18–1, that is, in the zones *IIA*, *IIB*, *IIIA*, and *I* where the flow rates where recalculated (Table 2). When both the circulation and bed lines are neglected, the effects of both lines are summed.

The effect of the bed and circulation lines is mainly noted in the raffinate outlet position (FIP = 18). In the absence of circulation lines, the *p*-x concentration in the raffinate increases, whereas the elimination of the bed lines produces the opposite effect.

Figure 8 shows the evolution of the extract concentrations for the case where the bed lines were eliminated (and, consequently, the primary and secondary flush streams). In Figure 8a, the average *p*-x and *p*-deb concentrations per switching interval for the case with bed lines installed are compared with the instantaneous and average concentrations obtained without bed lines. By comparing Figures 3c and 8b, it is observed that the absence of bed lines increases the amount of *p*-x collected in the extract per switching interval. In the presence of bed lines, the whole switching interval is effectively used to withdraw the product, whereas in the presence of bed lines, a fraction of the switching interval is used to displace the volume of fluid held back in the line. The influence of the circulation lines is again observed in Figure 8b, where it compares how the extract concentration taken from the first and last columns of one of the adsorbent chambers varies along a switching interval under CSS.

Table 3 summarizes the performance metrics of the unit obtained with and without circulation lines and with or without bed lines. The bed lines change slightly the product purity, as their volume influences the delay between the beginning of the step and the appearance of *p*-x at the outlet position of the rotary valve; this is also the time taken to displace the desorbent that fills the lines at the beginning of the step. Consequently, the amount of each component withdrawn per step changes slightly, because in the column preceding the extract port, the concentration decreases differently between components. Of course it is more apparent that the length of the bed lines alters the specific productivity (quantity of *p*-x obtained per unit of adsorbent and time).

Table 2. Plant Operation Information with Different Volumes for the Bed Lines (V_{line} is in m^3, t^* in s, and all Other Parameters in m^3/h)

V_{line}	0.225	0.169	0.113	0.056	0
A	67.92	67.92	67.92	67.92	67.92
W	338.4	338.4	338.4	338.4	338.4
L_I	504.6	502.1	499.7	497.2	494.7
L_{IIA}	402.5	400.0	397.5	395.0	392.6
L_{II}	392.6	392.6	392.6	392.6	392.6
L_{IIB}	384.9	386.6	388.4	390.5	392.6
L_{III}	444.3	444.3	444.3	444.3	444.3
L_{IIIA}	454.3	451.8	449.3	446.8	444.3
L_{IV}	314.6	314.6	314.6	314.6	314.6
Q_F	102.1	102.1	102.1	102.1	102.1
Q_D	139.6	137.2	134.7	132.2	129.7
Q_X	8.39	6.30	4.21	2.09	0
Q_H	9.91	7.44	4.98	2.47	0
Q_E	60.17	58.09	56.00	53.87	51.79
Q_R	190.0	187.5	185.0	182.5	180.1
t^*	106.3	106.3	106.3	106.3	106.3

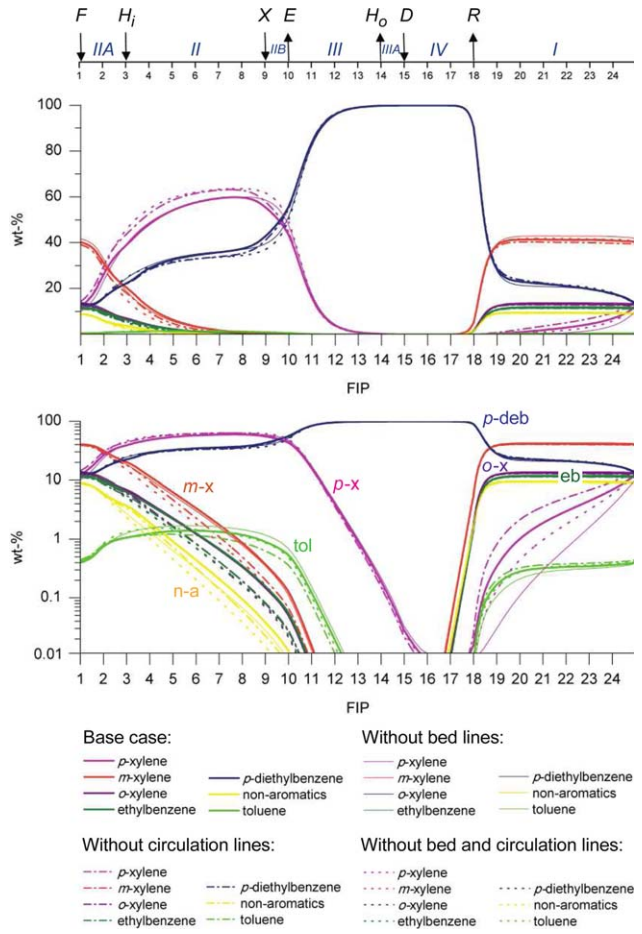

Figure 7. Concentration profiles (in the pump-around line) as function of the FIP for the base case and three variations: without circulation lines, without bed lines (model reduction to a four-zone configuration), and without bed lines and circulation lines (model reduction to a four-zone configuration).

[Color figure can be viewed in the online issue, which is available at wileyonlinelibrary.com.]

As the lengths of the circulation and bed lines influence the performance of the unit, it is of interest to analyze the variation of the performance parameters with the lengths of the circulation and bed lines; Figure 9 shows the variation of purity, recovery, desorbent consumption, and productivity. It is important to note that the variation of the length of the bed lines implies the recalculation of the zone flow rates as it was already explained before (Table 2).

The results presented in Figure 9 show that the purity requirements are achieved for a length of approximately 18.8 m. For this length, the recovery is 97%, the desorbent consumption is 7.7 kg of *p*-deb per kg of *p*-x in the extract, and the productivity is 69.6 kg of *p*-x per hour per cubic meter of adsorbent.

It is worth pointing out that the existence of bed lines is a consequence of the industrial implementation of the SMB unit with a rotary valve; the elimination of bed lines is only a hypothetical case. Nevertheless, the type of results presented in Figure 9 can be used for designing SMB industrial units.

Finally, the size of the dead volume created by the presence of internals was varied by ±2% and its effect is shown in Figures 10 and 11. These figures show that the bed-head dead volume influences significantly the performance of the industrial unit. Silva et al.[20] showed that the correct equivalence rules between the TMB and a SMB with nonnegligible bed-head dead volumes is

$$Q_s = \frac{(1-\varepsilon_b)V_c}{t^*}, \quad m_j = \frac{Q_j^{TMB}}{Q_s} = \frac{Q_j^{SMB}}{Q_s} - \frac{\varepsilon_b + \varepsilon_b'}{1-\varepsilon_b} \qquad (1)$$

where j the zone index, V_c the column volume, Q_s the volumetric flow rate of countercurrent moving solid in the TMB, t^* the switching interval of the SMB, Q_j^U the volumetric flow rate of fluid in zone j of unit U, ε_b the bed porosity, and $\varepsilon_b' = V_{bh}/V_c$ a measure of the bed-head dead volume (V_{bh}) with respect to the column volume; the m_j parameters represent the ratios of fluid to solid volumetric flow rates and are the standard variables used to define the region of complete separation in the framework of the equilibrium theory.[33–35] The formulas above show that the magnitude of ε_b' has a direct impact on the m_j parameters and, consequently, on the location of the operating point with respect to the boundaries of the separation region.

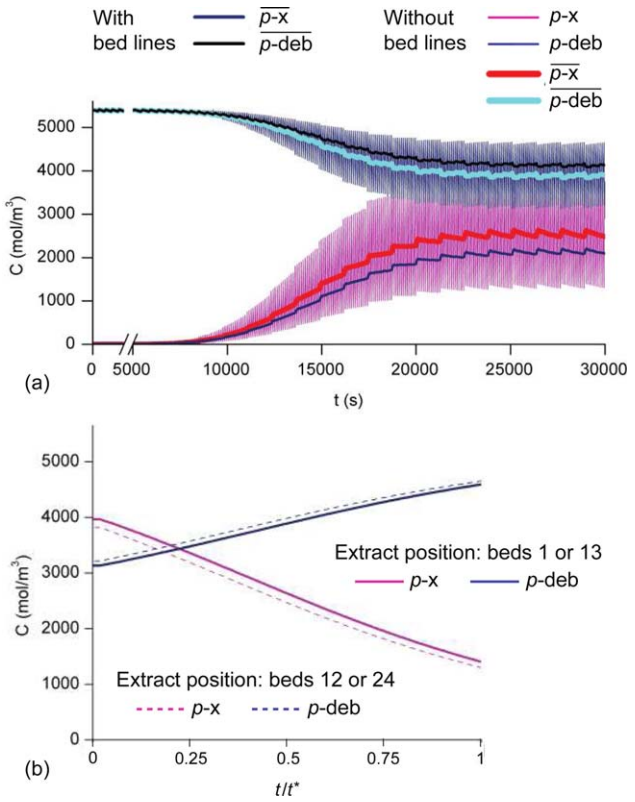

Figure 8. Extract concentrations (mol/m^3) as function of time for the case without bed lines (four-zone configuration): (a) evolution until CSS is achieved and comparison between the t^*-average concentrations; (b) concentration history in the extract during a switching interval (in CSS), t/t^*, for different positions of the extract in the adsorbent chamber and without bed lines: beds 1 or 13 and beds 12 or 24.

[Color figure can be viewed in the online issue, which is available at wileyonlinelibrary.com.]

Table 3. Performance Parameters when the Parex Unit is Operated with Seven Zones and with Four Zones (Limiting Case of Zero-Length Bed Lines); DC is Expressed as kg of *p*-Diethylbenzene per kg of *p*-Xylene Obtained in the Extract; PR is Given in kg of *p*-Xylene Obtained in the Extract per Hour and per m^3 of Adsorbent

	Seven Zones		Four Zones	
	With Circulation Lines	Without Circulation Lines	With Circulation Lines	Without Circulation Lines
PUX^E_{p-x} (%)	99.64	99.82	99.74	99.88
REX^E_{p-x} (%)	97.69	94.34	100	98.90
DC	7.61	7.79	6.48	6.55
PR	69.98	68.36	82.14	81.35

Table 4 lists the purity and recovery results obtained when the bed-head dead volume is varied by ±2% for the operating conditions of the case study taken from the industrial plant (first column of data in Table 2). The reduction of the dead volume between beds improves the product purity but reduces the *p*-x recovery because it increases the values of all the m_j parameters (i.e., the values of flow the rates Q_j^{TMB} for a fixed value of Q_s in an equivalent TMB without dead volumes) and, thus, moves the internal composition profile in the direction of the fluid flow, which reduces the trailing contamination in the extract but enriches the raffinate with a little more of the leading part of the *p*-x concentration front. The relative impact of these two opposing effects depends on the position of the concentration fronts.

As discussed above, the Parex cycle is not exactly t^*-periodic because the pump-around and push-around lines are connected to specific columns. However, the results shown so far suggest that the time-averaged concentration profiles do not change significantly if the small time lag introduced by the two circulation lines of the industrial Parex unit is neglected.

Besides the feed, desorbent, extract, and raffinate, three more streams are considered in the industrial Parex unit: flush in, flush out, and secondary flush (recycle). The secondary flush is a split from the main desorbent stream and, therefore, they both have the same composition. The flush-out stream is withdrawn at one predefined port and bed line and is immediately injected into the bed line corresponding to the flush-in position. If the seven-zone Parex configuration is simplified to a four-zone SMB, the wash percentage of the primary and secondary flushes can be set to zero.

Using these simplifying assumptions, it is possible to develop a rather detailed model of the Parex unit that considers the operation of the unit over a single switching interval as opposed to over a full cycle. This model, which is described in Appendix B, retains all of the essential properties of the full Parex model—including the bed-head dead volumes and bed

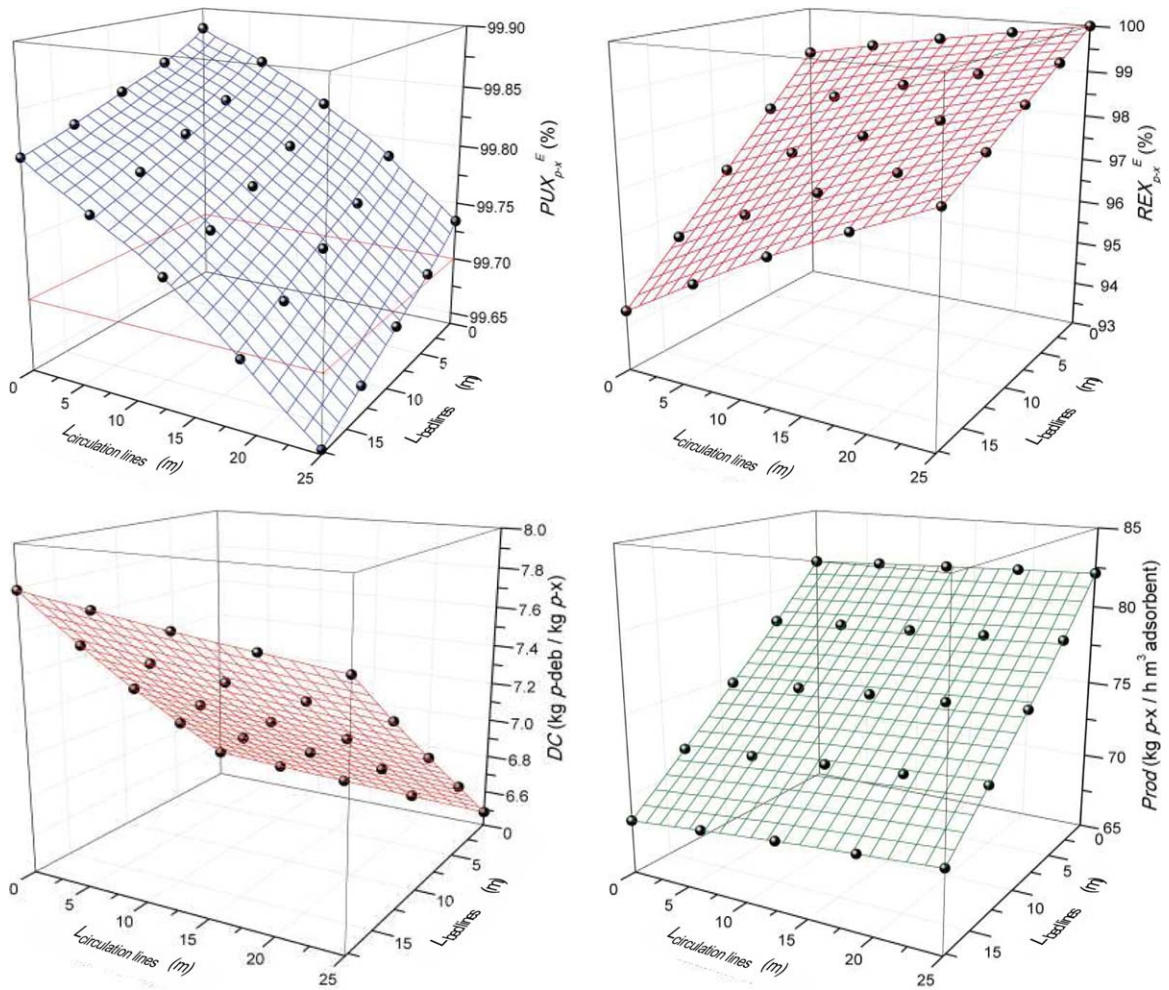

Figure 9. Performance parameters as function of the lengths of the bed and circulation lines.

[Color figure can be viewed in the online issue, which is available at wileyonlinelibrary.com.]

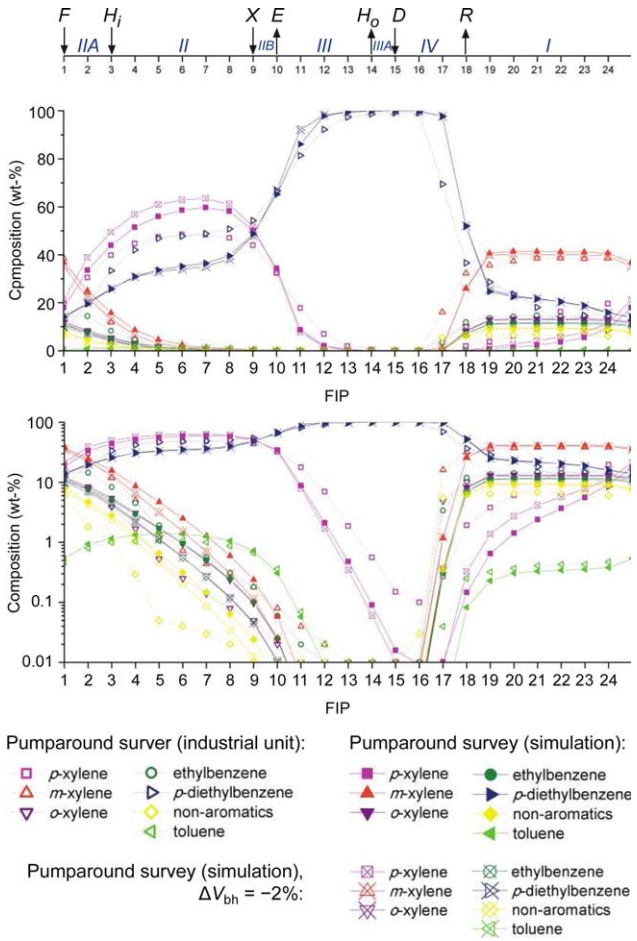

Figure 10. Concentration profiles (wt %) measured in the pump-around line as a function of the Feed Inlet Position (FIP): industrial data, simulation results, and simulation results for a bed-head dead volume 2% smaller.

[Color figure can be viewed in the online issue, which is available at wileyonlinelibrary.com.]

lines—but is computationally much more efficient because its CSS solution can be efficiently computed using a full-discretization approach. Although this approach has been previously used in simpler SMB models with a small number of columns,[37–40] it was never applied to the industrial-scale, 24-column Parex process.

Instead of moving the inlet and outlet nodes by one column in the direction of the fluid flow at the end of a switching interval, as in the full Parex model, in Appendix B, the nodes are fixed in space and the columns move upstream by one position at the end of a switching interval. This change in the observer's frame of reference makes it straightforward to simultaneously specify not only the closure equations that model the column switching but also the t^*-periodic boundary condition at CSS

$$\phi_{ij}(x, t=0) = \phi_{i,j+1}(x, t=t^*) \;\forall\; i, j, 0 \le z \le L_c \qquad (2)$$

Here, $i=1,\ldots,\ N_c$ is the component index, $j=1,\ldots,\ 24$ the column number, z the axial coordinate along a column, and ϕ_{ij} the vector of variables (fluid- and adsorbed-phase concentrations) that define the state of component i in column column j; Eq. 2 implicitly assumes that $j=25$ actually means $j=1$ (column 1 follows column 25 in the closed ring of columns).

The partial differential equations were discretized in both space and time using orthogonal collocation in finite elements for the space domains ($0 \le z \le L_c$) and Radau collocation for the time domain ($0 \le t \le t^*$). This problem was formulated numerically in AMPL[41] (http://ampl.com). The column lengths and bed lines were discretized using third-order orthogonal collocation on six finite elements and the time domain (switching interval) was discretized using third-order Radau collocation on 10 finite elements. The resulting large-scale, sparse nonlinear system of algebraic equations was solved using Ipopt,[42] version 3.11.2 (https://projects.coin-or.org/Ipopt), coupled to the Watson Sparse Matrix Package,[43] version 13.6.10 (http://www.research.ibm.com/projects/wsmp), parallelized over eight Intel Xeon processors. Ipopt implements a primal-dual interior-point method and uses line searches based on filter methods; it directly exploits first and second derivative (Hessians) information provided by AMPL via automatic differentiation. Although Ipopt is an efficient nonlinear optimizer, it was used here just as a nonlinear solver.

Consider the case study taken from the industrial plant (first column of data in Table 2). A set of m_j parameters that gives

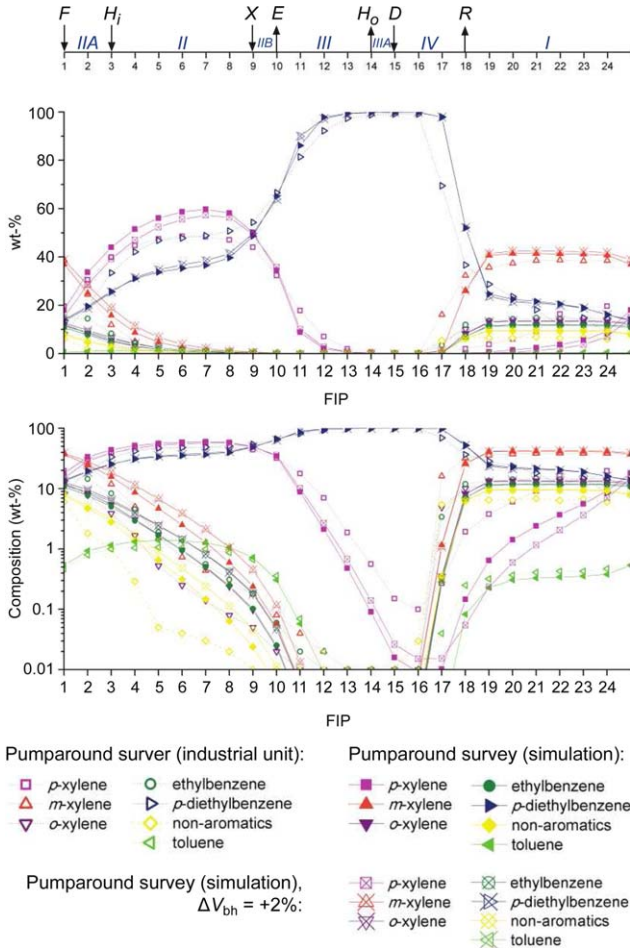

Figure 11. Concentration profiles (wt %) measured in the pump-around line as a function of the Feed Inlet Position (FIP): industrial data, simulation results, and simulation results for a bed-head dead volume 2% larger.

[Color figure can be viewed in the online issue, which is available at wileyonlinelibrary.com.]

Table 4. Purity and Recovery Considering a Variation of the Bed-Head Dead Volume, V_{bh}, of ±2%

	V_{bh} (m^3)	PUX^E_{p-x} (%)	REX^E_{p-x} (%)
−2% V_{bh} (Figure 10)	3.08	99.83	95.56
Base case	3.15	99.64	97.69
+2% V_{bh} (Figure 11)	3.21	99.26	99.15

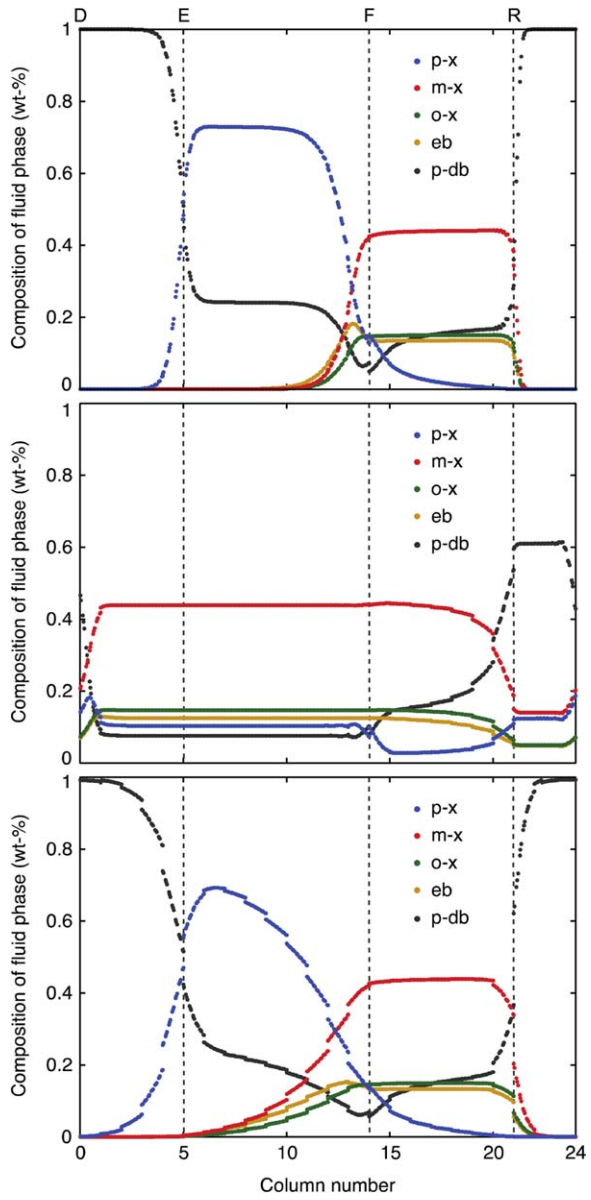

Figure 12. Axial concentrations profiles along the ring of 24 columns of the Parex unit measured at the middle of the switching interval under CSS conditions for three different scenarios: no bed-head dead volumes (top graph; $\epsilon'_b=0$, $PUX^E_{p-x}=99.9\%$, $REX^E_{p-x}=99.7\%$), bed-head dead volumes with uncorrected zone flow rates (middle graph; $\epsilon'_b=0.24$, $PUX^E_{p-x}=12.8\%$, $REX^E_{p-x}=17.7\%$) and bed-head dead volumes with corrected zone flow rates given by Eq. (1) (bottom graph; $\epsilon'_b=0.24$, $PUX^E_{p-x}=98.8\%$, $REX^E_{p-x}=99.0\%$).

[Color figure can be viewed in the online issue, which is available at wileyonlinelibrary.com.]

complete separation of *p*-xylene from the other xylenes and ethylbenzene in the feed mixture if the columns do not have bed-head dead volume ($\epsilon'_b=0$) is $m_I=1.037$, $m_{II}=0.467$, $m_{III}=0.657$, and $m_{IV}=0.217$. The top graph of Figure 12 shows the axial concentrations profiles along the ring of 24 columns measured at the middle of the switching interval under CCS conditions; the *p*-xylene purity and recovery are, respectively, $PUX^E_{p-x}=99.9\%$, $REX^E_{p-x}=99.7\%$.

Now, consider the case with bed-head dead volumes with $\epsilon'_b=0.24$, as in the industrial case. If the m_j values are not changed to account for the effect of the presence of the extra fluid in the bed-head dead volumes, the obtained axial concentrations profiles are those plotted in the middle graph of Figure 12. In this case, the *p*-xylene purity and recovery are $PUX^E_{p-x}=12.8\%$ and $REX^E_{p-x}=17.7\%$, respectively.

The zone flow rates can be corrected for the presence of the bed-head dead volume by means of Eq. 1, which is rewritten here as

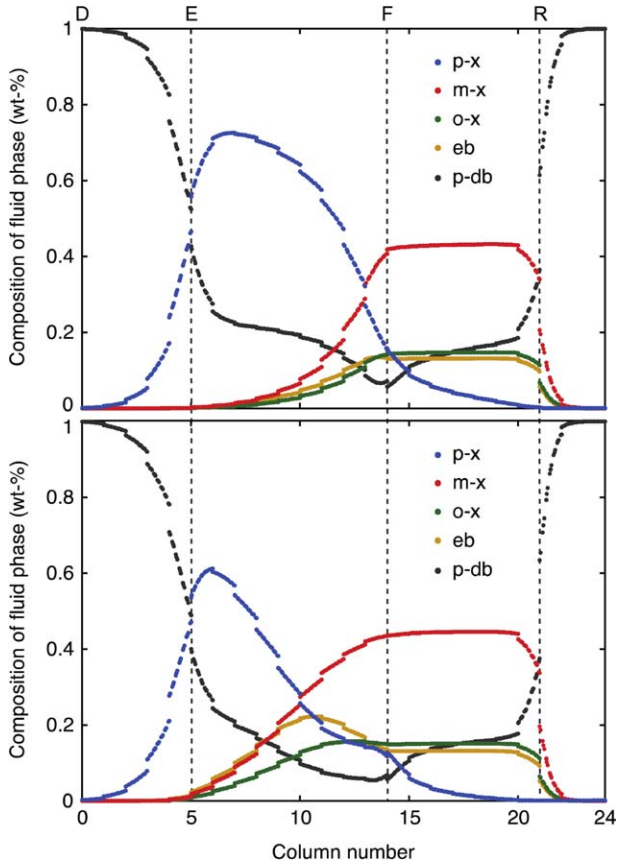

Figure 13. Axial concentrations profiles along the ring of 24 columns of the Parex unit measured at the middle of the switching interval under cyclic steady-state conditions for −2% (top; $PUX^E_{p-x}=99.3\%$, $REX^E_{p-x}=98.0\%$) and +2% (bottom; $PUX^E_{p-x}=93.3\%$, $REX^E_{p-x}=99.1\%$) variations of ϵ'_b around its nominal value of 0.24; $m_I=0.98$, $m_{II}=0.41$, $m_{III}=0.60$, and $m_{IV}=0.16$;; the zone flow rates were corrected for the effect of the bed-head dead volumes by Eq. 1 using the nominal value of ϵ'_b.

[Color figure can be viewed in the online issue, which is available at wileyonlinelibrary.com.]

$$t^*Q_j = \left[\left(\epsilon_b + \epsilon_b'\right) + (1-\epsilon_b)m_j\right]V_c \quad (3)$$

Using Eq. 3, the adjusted values of the flow rates change from $t^*Q_j/V_c = 0.791, 0.675, 1.023, 0.523$ ($j=1,\cdots,4$) to $t^*Q_j/V_c = 1.032, 0.916, 1.264, 0.764$. The corresponding axial concentration profiles are plotted in bottom graph of Figure 12. It is seen that the obtained purity and recovery values, $PUX^E_{p-x}=98.8\%$ and $REX^E_{p-x}=99.0\%$, are nearly recovered to their original values.

It is quite straightforward to use this model for assessing the effect of the size of the dead volume created by the presence of internals on the performance of the Parex unit for changes of ϵ_b' around its design value. For example, Figure 13 shows the results obtained when ϵ_b' is varied by $\pm 2\%$ around its design value of 0.24.

As discussed above, a slight reduction of the bed-head dead volume may improve the product purity but reduces the *p*-x recovery because it moves the internal composition profile in the direction of the fluid flow. It can happen that a small decrease in the bed-head dead volume remove traces of the final portion of the left edges of the *m*-x and *o*-x concentration fronts away from the extract port, thus improving the extract purity. But, given that the composition profile is moved in the direction of the fluid flow, it can also happen that the final portion of the right edge of the *p*-x concentration front contaminate the raffinate, thus reducing the *p*-x recovery. The relative impact of these two opposing effects depends on how far from the two outlet ports are the edges of the concentration fronts. Nevertheless, it is obvious that the performance of the Parex unit can always be improved when the dead volume is reduced but provided that the zone flow rates are correctly readjusted.

Conclusions

The effect of the different dead volumes on the performance of an industrial-scale Parex unit was studied by detailed simulation. The impact of the bed lines on the extract history was analyzed first. During the initial V_{line}/Q_E time units of each switching interval, the extract has the same composition as the desorbent. If the desorbent contains impurities, they propagate into the extract stream. When the unit is designed with a smaller dead volume in the bed lines, the recovery of the unit increases (for the same set of operating parameters) as more *p*-x is recovered per switching interval.

The design of a SMB unit with two circulation lines divides the 24 columns into two adsorbent chambers with 12 columns each. The simulations show that the existence of circulation lines changes the periodicity of the average concentration of each component in the extract from t^*-periodic to $12t^*$-periodic. The CSS of the Parex unit can thus be defined by the repetition of 12 switching intervals between Ports 1 (or 13) and 12 (or 24).

In terms of unit design, the volumes of bed and circulation lines affect the performance of the unit. Before studying the effect of the volume of these lines, it was verified that the level of axial dispersion considered for the bed lines affects the purity of the final product.

Using one of the cases from the industrial plant, the lengths of the circulation and bed lines were varied and their impact on the performance of the unit was assessed. The increase of the volume of the circulation lines increases the recovery and productivity, but reduces the purity and the desorbent consumption. The introduction of the bed lines and correspondent correction of flow rates reduces the purity and recovery of the unit.

It was further demonstrated that the dead volume created by the existence of internals between beds affects the performance of the unit. The reduction of these volumes increased the purity (for the operating parameters of Table 1).

It was also shown that if the small time lags introduced by the pump-around and push-around lines, which prevent the Parex unit from being exactly t^*-periodic, are neglected, it is possible to develop a detailed process model that considers the operation of the Parex unit over a single switching interval as opposed to a full cycle, and whose CSS solution can be efficiently computed using a full-discretization approach.

The results presented in this work show that the dead volumes, as well as the level of axial dispersion considered in these volumes, influence the performance of the industrial-scale unit, that is, the size of the dead volumes is large enough to interfere with the performance of the unit.

Acknowledgment

Marta S.P. Silva gratefully acknowledges the financial support from *Fundação para a Ciência e Tecnologia* (Ministry of Science and Technology of Portugal) for her Ph.D. scholarship SFRH/BDE/33836/2009.

Notation

A = rate of simulated circulation of the selective adsorbent pore volume, m^3/h
A_c = cross-sectional area of the column, m^2
BTX = benzene, toluene, xylenes
C = bulk liquid concentration, mol/m^3
CSS = cyclic steady state
D = diameter, m
DC = desorbent consumption, kg of *p*-deb/kg of *p*-x obtained in the extract
EOP = extract outlet position
$f_F^a = Q_F^a/Q_F$
$f_F^{\text{project}} = Q_F/Q_F^{\text{project}}$
f_H^{line} = fraction of the bed line washed by the primary flush stream
f_X^{line} = fraction of the bed line washed by the secondary flush (or recycle) stream
FIP = feed inlet position
H_i = primary flush-in stream
H_o = primary flush-out stream
k = overall mass-transfer coefficient, s^{-1}
K = Langmuir constant, m^3/mol
L = length, m
L_I = flow rate of zone *I*, m^3/h
L_{II} = flow rate of zone *II*, m^3/h
L_{IIA} = flow rate of zone *IIA*, m^3/h
L_{IIB} = flow rate of zone *IIB*, m^3/h
L_{III} = flow rate of zone *III*, m^3/h
L_{IIIA} = flow rate of zone *IIIA*, m^3/h
L_{IV} = flow rate of zone *IV*, m^3/h
$L_2 = L_{II} - W$
$L_3 = L_{III} - W$
$L_4 = L_{IV} - W$
Pe = Péclet number
PR = productivity, kg of $p-$x obtained in the extract/h m^3 of adsorbent
PUX = purity, %
Q = flow rate, m^3/h
q_m = saturation capacity, mol/kg of adsorbent
R_p = pellet radius, m
REX = recovery, %
SMB = simulated moving bed
t = time, s
t^* = switching time, s
TMB = true moving bed
u = interstitial velocity, m/s

u_{solid} = solid interstitial velocity, m/s
V = volume, m^3
V_s = selective volume, m^3
V_w = nonselective volume, m^3
W = rate of simulated circulation of the nonvolume, m^3/h

Greek symbols

ε_b = bulk porosity, V_b/V_c
ε_p = particle macroporosity, V_p/V_{ads}
ρ_p = apparent density, kg/m^3

Subscripts and superscripts

a = aromatic fraction
c = column
circ = circulation line
D = desorbent sream
dead = dead volume
E = extract stream
F = Feed stream
H = primary flush stream
line = bed line
R = raffinate stream
X = recycle or secondary flush stream

Abbreviations

p-x = *p*-xylene
m-x = *m*-xylene
o-x = *o*-xylene
eb = ethylbenzene
p-deb = *p*-diethylbenzene
n-a = nonaromatics
tol = toluene
benz = benzene

Literature Cited

1. Fabri J, Ulrich G, Simo TA. *Xylenes, Ullmann's Encyclopedia of Industrial Chemistry (Electronic Edition)*. Weinheim: Wiley-VCH Verlag, 2012.
2. Cannella WJ. *Xylenes and Ethylbenzene*. New York: Wiley, 2007.
3. Laurich S. p-Xylene Process. US Patent 3,467,724, Chevron Research Co., 1969.
4. Desideri RJ, Hirsig AR, Dresser T, Edison RR, Peterman LG, Truitt RE. Pure p-xylene by single stage. *Hydrocarbon Process.* 1974;53:81–83.
5. McKay DL, Goard HW. Continuous fractional crystallization. *Chem Eng Prog*. 1965;61:99–104.
6. Ockerbloom NE. Xylenes and higher aromatics. 1. Sources, specifications, producers, uses and outlook. *Hydrocarbon Process*. 1971;50:112–114.
7. Broughton DB, Neuzil RW, Pharis JM, Brearley CS. The parex process for recovering paraxylene. *Chem Eng Prog*. 1970;66(9):70–75.
8. Ash GA, Dao NQ, Gloyn AJ, Haritatos NJ, Hodgen PI, MacPherson SR, Morrison SG, Nacamuli GJ, Spindler PM, Thom BJ, Weber EP, Wolpert R. *Process for converting hydrocarbon feed to high purity benzene and high purity paraxylene. US Patent 6,004,452*, Chevron Chemical Company LLC, 1999.
9. Ash G, Barth K, Hotier G, Mank L, Renard P. ELUXYL: a new paraxylene separation process. *RevInst Fr Pétrole* 1994;49(5):541–549.
10. Otani S, Iwamura T, Sando K, Kanaoka M, Matsumura K, Akita S, Yamamoto T, Takeuchi I, Tasuaki T, Yoshio N, Mori T. *Separation process of components of feed mixture utilizing solid sorbent. US Patent 3,761,533*, Toray Industries, Japan, 1973.
11. *Par-Isom™ Process.* UOP LLC, 2007. Available at: www.uop.com.
12. Broughton DB, Gerhold CG. *Continuous sorption process employing fixed bed of sorbent and moving inlets and outlets. US Patent 2,985,589*, Universal Oil Products Company, 1961.
13. Broughton DB. *Fluid distributing means for packed chambers. US Patent 3,214,247*, Universal Oil Products Company, 1965.
14. Carson DB, Purse FV. *Rotary valve. US Patent 3,040,777*, Universal Oil Products Company, 1962.
15. Carson DB. *Flow distribution apparatus. US Patent 3,789,989*, Universal Oil Products Company, 1974.
16. Neuzil RW. *Aromatic hydrocarbon separation by adsorption. US Patent 3,558,730*, Universal Oil Products Company, 1971.
17. Broughton DB, Bieser HJ, Persak RA. Sixty years of sorbex operations. In: UOP Process Division Technology Conference. UOP Process Division, Des Plaines, IL, 1975.
18. Minceva M, Rodrigues AE. Understanding and revamping of industrial scale SMB units for p-xylene separation. *AIChE J*. 2006;53(1):138–149.
19. Johnson JA. UOP Sorbex Family of Technologies. In: Meyers RA, editor, *Handbook of Petroleum Refining Processes*, 3rd ed., New York, NY: McGraw-Hill, 2004.
20. Silva MSP, Mota JPB, Rodrigues AE. Modelling and simulation of an industrial scale parex process. *AIChE J*. 2015;61(4):1345–1363.
21. Pais LS, Loureiro JM, Rodrigues AE. Modeling strategies for enantiomers separation by SMB chromatography. *AIChE J*. 1998;44(3): 561–569.
22. Minceva M, Rodrigues AE. Modeling and simulation of a simulated moving bed for the separation of p-xylene. *Ind Eng Chem Res*. 2002;41:3454–3461.
23. Gomes PS, Minceva M, Rodrigues AE. Operation of an industrial SMB unit for p-xylene separation accounting for adsorbent ageing problems. *Sep Sci Technol*. 2008;43:1974–2002.
24. Hidajat K, Ching CB, Ruthven DM. Numerical simulation of a semi-continuous counter-current adsorption unit for fructose-glucose separation. *Chem Eng J*. 1986;33:B55–B61.
25. Charton F, Nicoud RM. Complete design of simulated moving bed. *J Chromatogr A*. 1995;702:97–112.
26. Gomes PS, Minceva M, Rodrigues AE. Operation strategies for simulated moving bed in presence of adsorbent ageing. *Sep Sci Technol*. 2007;42:1–37.
27. Migliorini C, Mazzotti M. Simulated moving bed with extra-column dead volume. *AIChE J*. 1999;45(7):1411–1421.
28. Minceva M, Pais LS, Rodrigues AE. Cyclic steady state of simulated moving bed processes for enantiomers separation. *Chem Eng Process*. 2003;42:93–104.
29. Minceva M, Rodrigues AE. Two-level optimization of an existing SMB for p-xylene separation. *Comput Chem Eng*. 2005;29:2215–2228.
30. Minceva M, Rodrigues AE. Influence of the transfer line dead volume on the performance of an industrial scale simulated moving bed for p-xylene separation. *Sep Sci Technol*. 2003;38(7):1463–1497.
31. Silva MSP, Mota JPB, Rodrigues AE. Fixed-bed adsorption of aromatic C_8 isomers: breakthrough experiments, modelling and simulation. *Sep Purif Technol*. 2012;90:246–256.
32. Glueckauf E. Theory of chromatography: Part 10. – Formule for diffusion into spheres and their application to chromatography. *Trans Faraday Soc*. 1955; 51:1540–1551.
33. Storti G, Mazzotti M, Morbidelli M, Carra S. Robust design of binary countercurrent adsorption separation processes. *AIChE J*. 1993;39:471–492.
34. Mazzotti M, Storti G, Morbidelli M. Optimal operation of simulated moving bed units for nonlinear chromatographic separations. *J Chromatogr A*. 1997;769:3–24.
35. Mazzotti M. Equilibrium theory based design of simulated moving bed processes for a generalized Langmuir isotherm. *J Chromatogr A*. 2006;1126:311–322.
36. Silva MSP, Mota JPB, Rodrigues AE. Adsorption equilibrium and kinetics of the Parex's feed and desorbent streams from batch experiments. *Chem Eng Technol*. 2014;37:1541–1551.
37. Mota JPB, Araújo JMM. Single-column simulated-moving-bed process with recycle lag. *AIChE J*. 2005;51:1641–1653.
38. Araújo JMM, Rodrigues RCR, Mota JPB. Use of single-column models for efficient computation of the periodic state of a simulated moving-bed process. *Ind Eng Chem Res*. 2006;45:5314–5325.
39. Rodrigues RCR, Araújo JMM, Mota JPB. Optimal design and experimental validation of synchronous, asynchronous and flow-modulated, simulated moving-bed processes using a single-column setup. *J Chromatogr A*. 2006;1162:14–23.
40. Rodrigues RCR, Araújo JMM, Eusébio MFJ, Mota JPB. Experimental assessment of simulated moving bed and varicol processes using a single-column setup. *J Chromatogr A*. 2007;1142:69–80.
41. Fourer R, Gay DM, Kernighan BW. *AMPL: A Modeling Language for Mathematical Programming*, 2nd ed. New York: Brooks/Cole, 2003.
42. Wächter A, Biegler LT. On the implementation of a primal-dual interiorpoint filter line search algorithm for large-scale nonlinear programming. *Math Program*. 2006;106:25–57.
43. Gupta A. *WSMP: Watson Sparse Matrix Package*. IBM Research Report RC21886 (98462). New York, 2000.

Appendix A

This appendix and Ref. 20 provide a detailed description of a typical industrial-scale Parex unit for producing an extract stream enriched in *p*-x and a raffinate stream depleted of *p*-*x*.

The Parex process implements the SMB principle by means of a rotary valve that synchronously switches the ports in the direction of the fluid flow.

The commercial Parex unit uses 24 adsorbent beds divided into two chambers. Each adsorbent chamber has 12 beds and each bed is connected to the rotary valve, as depicted in Figure 1. The liquid circulates between the two adsorbent chambers through the push-around and pump-around lines, which connect, respectively, beds 12 (column 1) and 13 (column 2), and beds 24 (column 2) and 1 (column 1).

In the commercial Parex unit, the adsorbent beds are divided into seven zones, named *I, IIA, II, IIB, III, IIIA,* and *IV*, instead of the standard four zones, because the unit uses seven streams: three inlets—feed, desorbent, and flush in—and four outlets—extract, raffinate, flush out, and recycle/secondary flush. The existence of three extra zones is due to the fact that the same bed lines are used to inject and to withdraw streams, thereby generating dead volumes that would contaminate the streams flowing in those lines during the subsequent switching interval if no countermeasures were taken. To avoid these problems, three ports are added in the rotary valve for flushing streams (Figure 1). The three streams used for washing the lines are:

Primary flush-out. The separation of zones *II*/*III* and zones *III*/*IV* is done by, respectively, withdrawing the extract and injecting the desorbent streams. If the desorbent were injected directly through a line previously used to withdraw the extract, the desorbent stream would be contaminated with *p*-x, which would increase its quantity in the raffinate and consequently reduce the recovery of *p*-x in the unit. It is important to note that the reduction of *p*-x recovery in the Parex unit decreases the conversion in the isomerization reactor (Isomar unit) located downstream in the process. To decrease the contamination of the desorbent by the extract stream, the line that in the next switching time period will be used to inject the desorbent stream is washed by removing the volume (or a fraction of it) that is held back in the line and injecting it in zone *II* (zone of separation of *p*-x). As previously mentioned, the primary flush-out stream is taken from the bed that is immediately upstream of the desorbent injection port; this one-column zone between the primary flush-out port and the desorbent port is named zone *IIIA*.

Primary flush-in. As the primary flush stream, which is withdrawn at a position located between the extract and desorbent ports, contains *p*-x, it must be injected again into the unit, otherwise the recovery decreases. The primary flush stream is injected into zone *II*, between the feed and extract ports, more precisely, two columns ahead of the feed port. The primary flush also pushes into the column the feed volume that remained in the lines after injection, thereby avoiding the contamination of the extract and the loss of feed. The injection of the primary flush separates zones *II* and *IIA*.

Secondary flush or recycle. A secondary flush is injected between the primary flush injection and the extract port to guarantee that the line used to remove the extract is clean. The secondary flush or recycle is a small desorbent stream diverted from the main desorbent stream after passing through the filters of the desorbent. The secondary flush makes a second wash of the line that will be used to withdraw the extract, by filling it with *p*-deb, and, therefore, it guarantees that the extract is removed without any contamination. The secondary flush port separates zones *II* and *IIB* and is connected to the bed upstream of the extract port.

The rotary valve switches periodically and synchronously the seven inlet/outlet ports of the unit in the direction of the fluid flow. The valve rotates by $360°/24 = 15°$ every switching interval, t^*, which is between 1 and 2 min depending on the operating conditions. The zone configuration of the Parex unit is 7-2-6-1-4-1-3 [*I*, *IIA*, *II*, *IIB*, *III*, *IIIA*, and *IV*] (the equivalent four-zone configuration would be 7-9-5-3).

The adsorbent chambers operate at 177°C and approximately 8.8 kg/cm^2. In the industrial-scale unit under study, the internal diameter of the adsorbent chambers is 4.267 m and the total height without the elliptical heads is 13.535 m (measured between the top of Section 1 or 13 and the bottom of Section 12 or 24). A section of the adsorbent chamber consists of an adsorbent bed, the grid and support grid beams, and the internal piping.

A detailed analysis of the dimensions of the internals shows that if the height of each section is measured between the bottom of the grids above and below each bed, the volume available for the adsorbent is equal in all beds, as is the dead volume created by the existence of internals.

The length of the push-around and pump-around lines can be estimated from the height of the adsorbent chamber without the heads, 13.535 m, the height of each head (top and bottom), 1.938 m, the distance between the inlet/outlet point and the side of the adsorbent chamber (adsorbent chamber radius), 2.134 m, and approximately 3 m for the distance between the adsorbent chambers. The volumes of the pipe distributors to the top grid and from the bottom grid are, approximately, 0.15 and 0.29 m^3; their length can be assumed equal to the height of each elliptical head. The length of the circulation lines is approximately 25 m. Table 1 summarizes the relevant dimensions of the industrial-scale Parex unit along with some adsorbent characteristics.

In the pump-around line, a pump-around controller keeps each zone flow rate constant as the zone moves around the adsorption circuit. The pump-around control is based on zone equations written as a function of the rotary valve position at any given time. The position of the rotary valve is usually defined by reference to the position of the feed stream. Because for all practical purposes the flowing liquid is incompressible, fixing the flow rate in one zone necessarily fixes the flow rates in all zones because at each inlet or outlet point, the zone flow rate downstream of that point is equal to the upstream flow rate plus or minus whatever flow rate is added or removed at that point.

Appendix B

The model of the 24-column industrial-scale Parex unit described in this Appendix is based on the schematic of an adsorbent chamber depicted in Figure 14.

The differential material balances in the interparticle fluid flowing through the packed beds can be written as

$$\frac{\partial C_{ij}}{\partial \theta}+\frac{1-\varepsilon_b}{\varepsilon_b}k_i\left(C_{ij}-\overline{c}_{ij}\right)=\frac{t^*Q_j}{\varepsilon_b V_c}\left(\frac{1}{Pe}\frac{\partial^2 C_{ij}}{\partial x^2}-\frac{\partial C_{ij}}{\partial x}\right),\ \forall\ 0<x<1,\quad 0<\theta\leq 1 \tag{B1}$$

where $i=1,\ldots,N_c$ is the component index, $j=1,\ldots,24$ the column number, $\theta=t/t^*$ a dimensional time coordinate, $x=z/L_c$ a dimensional axial coordinate, C_{ij} (mol/m^3) the concentration in the bulk of the interparticle fluid, $\overline{c}_{ij}$ (mol/m^3) the average fluid-phase concentration in the macropore volume of the pellets, Q_j (m^3/s) the volumetric flow rate, k_i (s^{-1}) the linear-driving-force (LDF) mass-transfer coefficient, Pe the Péclet number for axial dispersion, ε_b the interparticle porosity, and V_c the column volume.

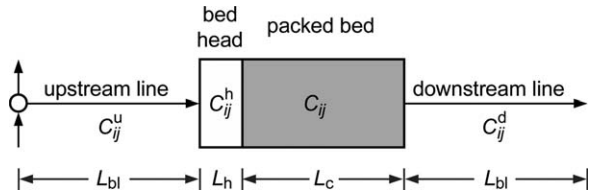

Figure 14. Simplified schematic of an adsorbent chamber: bed head, packed bed, injection/withdrawal node, and bed lines.

The material balances in the zeolite pellets are given by[36]

$$\varepsilon_p \frac{\partial \overline{c}_{ij}}{\partial \theta} + \rho_p \frac{\partial \overline{q}_{ij}^{*}}{\partial \theta} = t^* k_i \left(C_{ij} - \overline{c}_{ij}\right), \ \forall\ 0 \le x \le 1, \quad 0 < \theta \le 1 \tag{B2}$$

where $\overline{q}_{ij}^{*}$ (mol/kg of adsorbent) is the average adsorbed concentration of the ith component in equilibrium with the intraparticle fluid with composition $\overline{c}_{ij}$, ε_p is the particle porosity, and ρ_p (kg/m^3) is the apparent density of the zeolite pellets.

The adsorption equilibrium is described by a multicomponent Langmuir-type isotherm[31]

$$\overline{q}_{ij}^{*} = \frac{q_{mi}\ K_i\ \overline{c}_{ij}}{1 + \sum_n K_n\ \overline{c}_{nj}} \tag{B3}$$

where the K_i (m^3/mol) are the Langmuir constants and the q_{mi} the saturation capacities expressed in mol/(kg of adsorbent).

Equation B1 is subjected to the following boundary conditions

$$\begin{cases} x=0: \ C_{ij} - \dfrac{1}{Pe}\dfrac{\partial C_{ij}}{\partial x} = C_{ij}^{h} \\ x=1: \ \dfrac{\partial C_{ij}}{\partial x} = 0 \end{cases} \quad \forall\ \theta > 0 \tag{B4}$$

where C_{ij}^{h} is the concentration in the bead-head dead volume, which is modeled as a continuous, perfectly mixed stirred tank.[20] The equation governing the dynamics of C_{ij}^{h} can be expressed as

$$V_h \frac{dC_{ij}^{h}}{d\theta} = t^* Q_j \left[\left(C_{ij}^{u}\right)_{x=1} - C_{ij}^{h}\right] \ \forall\ \theta > 0 \tag{B5}$$

where V_h is the volume of the bed-head.

A dispersed plug-flow model governs the flow through the upstream and downstream bed lines

$$\frac{\partial C_{ij}^{u/d}}{\partial \theta} = \frac{t^* Q_j}{V_{bl}} \left(\frac{1}{Pe_{bl}} \frac{\partial^2 C_{ij}^{u/d}}{\partial x^2} - \frac{\partial C_{ij}^{u/d}}{\partial x}\right), \ \forall\ 0 < x < 1, \quad 0 < \theta \le 1 \tag{B6}$$

Here, V_{bl} is the volume of the bed line and Pe_{bl} is the Péclet number for axial dispersion in the line; the superscript u/d denotes that the same type of equation applies to C_{ij}^{u} and C_{ij}^{d}.

The boundary conditions for the upstream bed line are written as

$$\begin{cases} x=0: \ Q_j\left(C_{ij}^{u} - \dfrac{1}{Pe_{bl}}\dfrac{\partial C_{ij}^{u}}{\partial x}\right) = \begin{cases} Q_{IV}\left(C_{i,24}^{d}\right)_{x=1} + Q_D C_i^{D}, & j=1 \\ Q_{II}\left(C_{i,14}^{d}\right)_{x=1} + Q_F C_i^{F}, & j=15 \\ Q_j C_{i,j-1}^{u}, & j \notin \{1,\ 15\} \end{cases} \\ x=1: \ \dfrac{\partial C_{ij}^{u}}{\partial x} = 0 \end{cases} \quad \forall\ \theta > 0 \tag{B7}$$

whereas those for the downstream bed line are given by

$$\begin{cases} x=0: \ C_{ij}^{d} - \dfrac{1}{Pe_{bl}}\dfrac{\partial C_{ij}^{d}}{\partial x} = \left(C_{ij}\right)_{x=1} \\ x=1: \ \dfrac{\partial C_{ij}^{d}}{\partial x} = 0 \end{cases} \quad \forall\ \theta > 0 \tag{B8}$$

For computational convenience, the countercurrent contact between the solid and fluid is simulated by moving the columns upstream by one position at the end of a switching interval while keeping the inlet and outlet nodes fixed in space. Using this formulation, the material balances at the two inlet nodes—fresh desorbent (concentration C_i^D) admixed at the upstream end of column 1 and fresh feed (concentration C_i^F) admixed at the upstream end of column 15—are easily incorporated into the left boundary condition of the upstream bed line, as given by Eq. B7. More importantly, however, is that this choice of the observer's frame of reference for the SMB unit makes it straightforward to simultaneously specify not only the closure equations that model the column switching but also the t^*-periodic boundary condition

$$\phi_{ij}(x, \theta=0) = \phi_{i,j+1}(x, \theta=1) \ \forall\ i,j, 0 \le x \le 1 \tag{B9}$$

where $\phi \in \left\{C, \overline{c}, C^{u}, C^{d}\right\}$, and

$$C_{ij}^{h}(\theta=0) = C_{i,j+1}^{h}(\theta=1) \ \forall\ i,j \tag{B10}$$

In these equations, it is implicitly assumed that $j=25$ actually means $j=1$ (column 1 follows column 25 in the closed ring of columns).

Manuscript received Feb. 8, 2015, and revision received Aug. 7, 2015.